

ARTICLE

Influence of Electron Donating Ability on Reverse Intersystem Crossing Rate for One Kind of Thermally Activated Delayed Fluorescence Molecules

Ming-lang Wang^{a,b}, Jian-zhong Fan^a, Li-li Lin^{a*}*a. Shandong Province Key Laboratory of Medical Physics and Image Processing Technology, School of Physics and Electronics, Shandong Normal University, Jinan 250014, China**b. Department of Electronics, Peking University, Beijing 100871, China*

(Dated: Received on October 19, 2017; Accepted on December 22, 2017)

First-principles calculations are applied for investigating influence of electron donating ability of donor groups in eight thermally activated delayed fluorescence (TADF) molecules on their geometrical structures and transition properties as well as reverse intersystem crossing (RISC) processes. Results show that the diphenylamine substitution in the donor part can slightly change the bond angle but decrease bond length between donor and acceptor unit except for the lowest triplet state (T_1) of carbazole-xanthone molecule. As the electron donating ability of donor groups is increased, the overlap between the highest occupied molecular orbital (HOMO) and the lowest unoccupied molecular orbital (LUMO) is decreased. As the diphenylamine groups are added in donor part, the delocalization of HOMO is enlarged, which brings a decreased energy gap ($\Delta E_{S_1-T_1}$) between the lowest singlet excited state (S_1) and T_1 state. Furthermore, with the calculated spin-orbit coupling coefficient (H_{so}), one finds that the larger value of $\frac{\langle S_1 | \hat{H}_{so} | T_1 \rangle^2}{\Delta E_{S_1-T_1}^2}$ is, the faster of RISC is. The results show that all investigated molecules are promising candidates as TADF molecules. Overall, a wise molecular design strategy for TADF molecules, in which a small $\Delta E_{S_1-T_1}$ can be achieved by enlarging the delocalization of frontier molecular orbitals with large separation between HOMO and LUMO, is proposed.

Key words: Thermally activated delayed fluorescence, Donating ability, Reverse intersystem crossing, Spin-orbit coupling

I. INTRODUCTION

Since the milestone work of Tang *et al.* in 1987, organic light-emitting diodes (OLEDs) have attracted extensive attentions because of their potential application in flat-panel display and solid-state lighting [1–3]. In OLEDs, the singlet to triplet exciton formation ratio is 1:3 due to the spin statistics. For normal fluorescence emitters, radiative decay of the triplet excitons that account for 75% is spin forbidden and only the singlet excitons (25%) can be used for light emitting. To realize the goal of fully harvesting the triplet excitons, phosphorescent materials are developed and have achieved great success [4–7]. However, the phosphorescent materials are limited to Ir and Pt complexes, thus both fluorescence and phosphorescence OLEDs have advantages and disadvantages. Recently, Adachi *et al.* successfully achieved 100% internal quantum efficiency (IQE) by the use of pure organic thermally activated

delayed fluorescence (TADF) OLEDs [8–12]. For effective TADF-OLEDs, a small energy gap ($\Delta E_{S_1-T_1}$) between the lowest singlet excited state (S_1) and lowest triplet excited state (T_1) is expected, which can be achieved by decreasing the overlap between highest occupied molecular orbital (HOMO) and lowest unoccupied molecular orbital (LUMO). According to the equation $K_{RISC} \approx \frac{1}{3} \exp\left(\frac{-\Delta E_{S_1-T_1}}{k_B T}\right)$, where k_B denotes the Boltzmann constant and T is temperature, a small $\Delta E_{S_1-T_1}$ can facilitate the reverse intersystem crossing (RISC) process [13]. For improving utilization of excitons, one effective way is to convert triplet excitons into singlet excitons through a rapid RISC process [14–16]. Moreover, the spin-orbit coupling coefficient H_{so} between S_1 and T_1 is also a key factor that influences the conversion rate, so two important factors H_{so} and $\Delta E_{S_1-T_1}$ should be determined for realizing high efficient RISC process.

As we know, molecular structures determine their photophysical properties. In order to illustrate the influence of modification in donor groups of TADF molecules on their transition properties, $\Delta E_{S_1-T_1}$, ISC and RISC rates, here we adopt the xanthone (XTN)

*Author to whom correspondence should be addressed. E-mail: linll@sdsu.edu.cn

which is well known for its involved solvent and temperature dependent photophysics as electron acceptor unit [17], the carbazole, phenoxazine (PXZ), 9,9-dimethyl-9,10-dihydroacridine (DMAC) and phenothiazine (PTZ) as well as their derivatives which is substituted by diphenylamine as electron donating part to construct carbazole-XTN (a), PXZ-XTN (b), DMAC-XTN (c), PTZ-XTN (d) as well as carbazole-II-XTN (e), PXZ-II-XTN (f), DMAC-II-XTN (g), PTZ-II-XTN (h), all studied structures are shown in FIG. 1. Thus, we can analyze the effect of different electron donating ability and delocalization of frontier molecular orbitals on $\Delta E_{S_1-T_1}$, ISC and RISC rates. Furthermore, we can determine the dominant factor in realizing efficient RISC process and provide some suggestions for designing high efficient TADF emitters.

II. COMPUTATION

The geometry optimizations and frequency calculations are performed for the ground and excited states by using density functional theory (DFT) and time-dependent density functional theory (TD-DFT) with the B3LYP functional and 6-31G(d) basis set respectively. No imaginary frequencies are found which can help one to ensure the structure is stabilized. All calculations are carried out by Gaussian 16 package [18]. Besides, we not only draw the distribution of HOMO and LUMO but also analyze the overlap between them by Multiwfn (a multifunctional wavefunction analyzer) [19]. Moreover, based on the analysis of the excitation component of S_1 state, the HOMO-LUMO dominates the transition for all studied molecules, so the distribution of HOMO (LUMO) can be represented by the distribution of hole (electron). Moreover, we analyze the delocalization of hole by the following equation $X_{\text{hole}} = \int x \rho^{\text{hole}}(r) dr$, where x is component of r . The root mean square deviation (RMSD) of hole is used to characterize its distribution breadth. Meanwhile, the coupling coefficients of $\langle S_1 | \hat{H}_{\text{so}} | T_1 \rangle$, $\langle S_1 | \hat{H}_{\text{so}} | T_2 \rangle$ and $\langle S_1 | \hat{H}_{\text{so}} | T_3 \rangle$ are calculated based on the optimized structures of T_1 , T_2 and T_3 respectively, all results can be acquired by Dalton 2013 package [20].

Finally, the intersystem crossing rate constant from initial singlet/triplet to triplet/singlet states can be calculated based on the perturbation theory as

$$K_{f \leftarrow i}^{\text{ISC}} = K_{f \leftarrow i}^{(0)} + K_{f \leftarrow i}^{(1)} + K_{f \leftarrow i}^{(2)} \quad (1)$$

Where

$$K_{f \leftarrow i}^{(0)} \equiv \frac{1}{\hbar^2} |H_{fi}^{\text{SO}}|^2 \int_{-\infty}^{\infty} dt e^{i\omega_{if}t} \rho_{fi}^0(t) \quad (2)$$

$$K_{f \leftarrow i}^{(1)} \equiv \text{Re} \left[\frac{2}{\hbar^2} \sum_k H_{fi}^{\text{SO}} T_{if,k} \int_{-\infty}^{\infty} dt e^{i\omega_{if}t} \rho_{fi,k}^1(t) \right] \quad (3)$$

$$K_{f \leftarrow i}^{(2)} \equiv \frac{1}{\hbar^2} \sum_{k,l} T_{if,k} T_{fi,l} \int_{-\infty}^{\infty} dt e^{i\omega_{if}t} \rho_{fi,kl}^2(t) \quad (4)$$

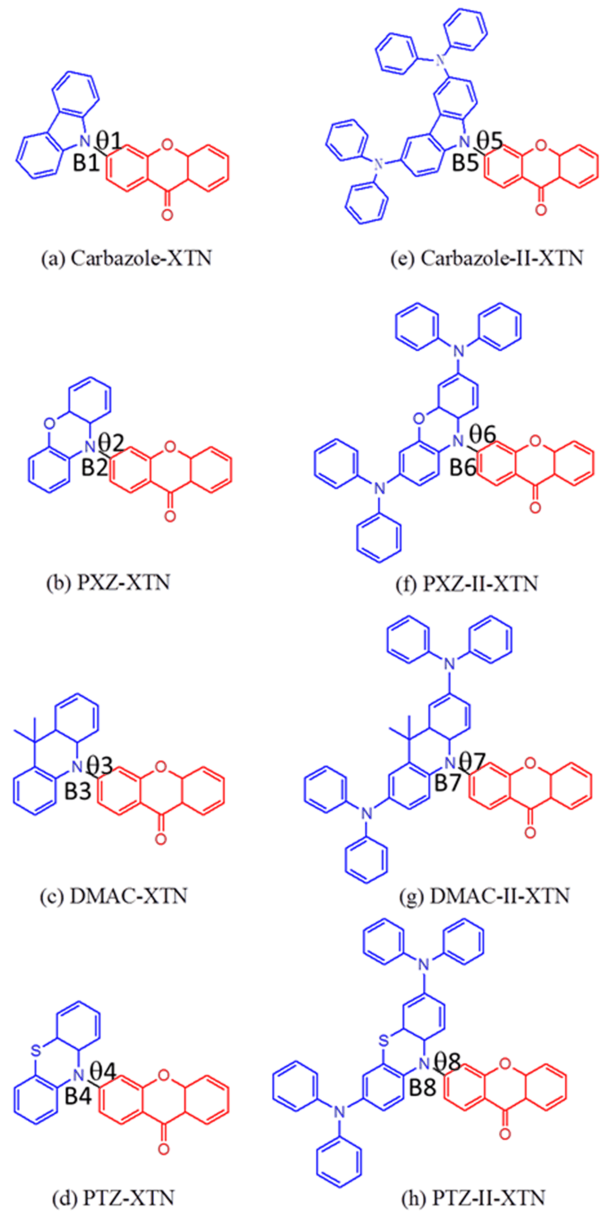


FIG. 1 Geometry structures of all studied molecules.

$T_{if,k(l)}$ is the mixed spin-orbit and non-radiative couplings between two electronic states for the $k(l)$ th normal mode [21, 22],

$$T_{if,k(l)} = \sum_n \left(\frac{H_{in}^{\text{SO}} \langle \phi_n | \hat{P}_{fk} | \phi_f \rangle}{\Delta E_{nf}} + \frac{H_{nf}^{\text{SO}} \langle \phi_i | \hat{P}_{nk} | \phi_n \rangle}{\Delta E_{in}} \right) \quad (5)$$

$$\rho_{fi,k}^1(t) = Z_i^{-1} \text{Tr}[\hat{P}_{fk} e^{-i\tau_f \hat{H}_f} e^{-i\tau_i \hat{H}_i}] \quad (6)$$

$$\rho_{fi,kl}^2(t) = Z_i^{-1} \text{Tr}[\hat{P}_{fk} e^{-i\tau_f \hat{H}_f} \hat{P}_{fl} e^{-i\tau_i \hat{H}_i}] \quad (7)$$

Eq.(6) and Eq.(7) are from Ref.[23] and Ref.[24] respectively.

For the first-order contribution $K_{f \leftarrow i}^{(0)}$, by applying the thermal vibration correlation function $\rho_{\text{IC}}(t, T)$, the

TABLE I Dihedral angle and bond length (marked out in FIG.1) between donor and acceptor for S_0 , S_1 and T_1 are listed respectively based on optimized structures.

| Geometry | Dihedral angle/(°) | | | Bond length/Å | | |
|------------------|--------------------|-------|-------|---------------|-------|-------|
| | S_0 | S_1 | T_1 | S_0 | S_1 | T_1 |
| Carbazole-XTN | 50.2 | 90.1 | 48.9 | 1.414 | 1.453 | 1.410 |
| PXZ-XTN | 99.6 | 89.9 | 89.8 | 1.429 | 1.461 | 1.460 |
| DMAC-XTN | 88.9 | 90.0 | 89.9 | 1.433 | 1.465 | 1.464 |
| PTZ-XTN | 81.6 | 90.0 | 90.0 | 1.436 | 1.466 | 1.465 |
| Carbazole-II-XTN | 49.4 | 89.6 | 89.6 | 1.412 | 1.450 | 1.449 |
| PXZ-II-XTN | 106.4 | 90.5 | 90.4 | 1.426 | 1.458 | 1.457 |
| DMAC-II-XTN | 88.8 | 90.2 | 90.2 | 1.433 | 1.461 | 1.460 |
| PTZ-II-XTN | 82.2 | 90.7 | 90.7 | 1.436 | 1.464 | 1.463 |

simplest and the most commonly employed intersystem crossing rate formalism can be written as:

$$K_{\text{ISC}} = \frac{1}{\hbar^2} \langle \phi_f | \hat{H}^{\text{SO}} | \phi_i \rangle \int_{-\infty}^{\infty} dt [e^{i\omega_{if}t} Z_i^- \rho_{\text{ISC}}(t, T)] \quad (8)$$

All these calculations for ISC and RISC rates are performed by MOMAP (molecular materials property prediction package) promoted by the Institute of Chemistry Chinese Academy of Sciences and Department of Chemistry in Tsinghua University. Both the methodology and application of this formalism can be found in Peng *et al*'s and Shuai *et al*'s. works [25–30].

III. RESULTS AND DISCUSSION

A. Geometry structures

According to the method discussed in computational details, the geometry structures of S_0 , S_1 and T_1 for all investigated molecules are optimized by B3LYP functional. Basic molecular structures are shown in FIG. 1 and the main geometric parameters are listed in Table I. One can see that different donor units change the dihedral angle and bond length (marked out in FIG. 1) between donor and acceptor for S_0 , S_1 and T_1 states. For a more visible comparison, FIG. 2 is plotted. Combining Table I and FIG. 2, the dihedral angle (θ) is almost unchanged for S_1 and T_1 states comparing all studied molecules except for carbazole-XTN, this indicates a small geometry variation when molecule changes from S_1 state to T_1 state. Meanwhile, the dihedral angles in S_0 , S_1 and T_1 states are similar for DMAC-XTN and DMAC-II-XTN, this illustrates a small change of reorganization energy from S_1 to S_0 and T_1 to S_0 . Besides, the bond length between donor and acceptor is slightly changed for S_1 and T_1 states compared all studied molecules except for molecule Carbazole-XTN. The bond length of all molecules in S_1 state is the longest one compared with molecules in S_0 and T_1 states, this indicates a decreased interaction between donor and acceptor unit for S_1 state. Moreover, comparing the bond

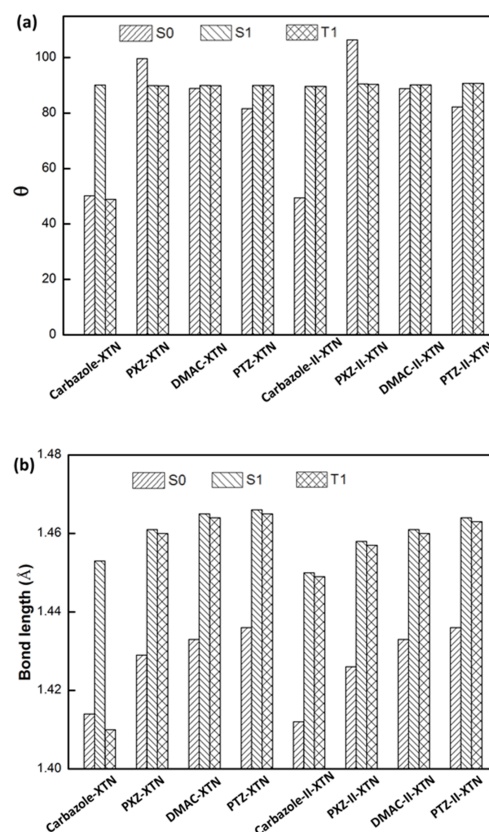


FIG. 2 Dihedral angles (a) and bond length (b) between donor and acceptor for optimized S_0 , S_1 and T_1 states of all studied molecules respectively.

length of the first four molecules with their diphenylamine substitutions in their S_0 , S_1 and T_1 states respectively, one can see that the latter four molecular bond lengths are reduced comparing with the former four molecules except for the T_1 states of carbazole-XTN and carbazole-II-XTN. All these results suggest that diphenylamine substitution can decrease the bond length between donor and acceptor unit while little effect on the dihedral angle between them.

TABLE II Atomic charges of investigated molecules in S_0 and S_1 using NPA method. Δ is the charge difference between S_1 and S_0 states.

| Geometry | | Natural charge | |
|------------------|----------|----------------|--------|
| | | Acceptor | Donor |
| Carbazole-XTN | S_0 | 0.171 | -0.171 |
| | S_1 | -0.486 | 0.486 |
| | Δ | -0.657 | 0.657 |
| PXZ-XTN | S_0 | 0.197 | -0.197 |
| | S_1 | -0.610 | 0.610 |
| | Δ | -0.807 | 0.807 |
| DMAC-XTN | S_0 | 0.196 | -0.196 |
| | S_1 | -0.641 | 0.641 |
| | Δ | -0.837 | 0.837 |
| PTZ-XTN | S_0 | 0.201 | -0.201 |
| | S_1 | -0.643 | 0.643 |
| | Δ | -0.844 | 0.844 |
| Carbazole-II-XTN | S_0 | 0.167 | -0.167 |
| | S_1 | -0.580 | 0.580 |
| | Δ | -0.747 | 0.747 |
| PXZ-II-XTN | S_0 | 0.186 | -0.186 |
| | S_1 | -0.596 | 0.596 |
| | Δ | -0.782 | 0.782 |
| DMAC-II-XTN | S_0 | 0.198 | -0.198 |
| | S_1 | -0.669 | 0.669 |
| | Δ | -0.867 | 0.867 |
| PTZ-II-XTN | S_0 | 0.200 | -0.200 |
| | S_1 | -0.663 | 0.663 |
| | Δ | -0.863 | 0.863 |

Moreover, the electron-donating ability affects molecular photophysical properties. Atomic charges of the S_0 and S_1 states for the eight molecules are calculated by natural population analysis (NPA) method, all data are collected in Table II. From Table II, charges of the donor group for the S_0 and S_1 states are negative and positive respectively for all studied molecules, while opposite results are found for the acceptor unit. In addition, the charge difference (Δ) between S_1 and S_0 is calculated, we use the value of Δ to measure the electron donating ability, the larger the charge difference is, the stronger the electron-donating ability is. Thus, we illustrate the effect of different electron-donating to $\Delta E_{S_1-T_1}$ and transition properties. Moreover, comparing the former four molecules and the corresponding ones with diphenylamine added in donor unit, the effect of delocalization of molecular orbital to photophysical properties can be analyzed.

B. Frontier molecular orbital properties

Composition of frontier molecular orbital (FMO) is closely related to the molecular excitation properties

TABLE III Overlap between HOMO and LUMO (S) as well as the value of RMSD of hole (δ_{hole}) and electron (δ_{electron}) with the unit of Å are listed.

| Geometry | S | δ_{hole} | δ_{electron} |
|------------------|--------|------------------------|----------------------------|
| Carbazole-XTN | 0.3483 | 2.960 | 3.031 |
| PXZ-XTN | 0.1699 | 2.590 | 2.888 |
| DMAC-XTN | 0.1192 | 2.687 | 2.864 |
| PTZ-XTN | 0.1101 | 2.560 | 2.858 |
| Carbazole-II-XTN | 0.2332 | 4.763 | 3.106 |
| PXZ-II-XTN | 0.1971 | 4.390 | 2.955 |
| DMAC-II-XTN | 0.0923 | 4.834 | 2.867 |
| PTZ-II-XTN | 0.0961 | 4.742 | 2.863 |

such as absorption and emission properties. Moreover, ultrafast excited state dynamics investigation is a research hotspot [31, 32]. In order to get a deep understanding of photophysical behavior of all investigated compounds, analysis of FMO at S_0 state is performed. Distributions of HOMO and LUMO as well as their energy levels are plotted in FIG. 3. One can see that the HOMO and LUMO are localized in donor and acceptor unit respectively, and small orbital overlap between HOMO and LUMO is found. According to the following equation

$$\Delta E_{S_1-T_1} = 2 \iint \phi_L(1) \phi_H(2) \frac{e^2}{r_{12}} \phi_L(2) \phi_H(1) dr_1 dr_2 \quad (9)$$

a small $\Delta E_{S_1-T_1}$ can be expected. Moreover, the delocalization of frontier orbitals should also be considered. It is reasonable to obtain the same overlap between the HOMO and LUMO for two different molecules such as, one which has the electronic density of both orbitals confined to one group of the molecule and a second for which the density of both orbitals is delocalized over the whole molecular scaffold. This degree of spatial confinement is important. Comparing molecule Carbazole-XTN (a) with carbazole-II-XTN (e), PXZ-XTN (b) with PXZ-II-XTN (f), DMAC-XTN (c) with DMAC-II-XTN (g) and PTZ-XTN (d) with PTZ-II-XTN (h), one can see that the energy of LUMO is almost unchanged while the energy of HOMO is increased, which brings a decreased HOMO-LUMO energy gap for later four molecules. Moreover, the diphenylamine in donor part not only adjusts the HOMO-LUMO energy level but also increases the delocalization of HOMO. In order to achieve quantitative comparison, the index of S , δ_{hole} and δ_{electron} are used to characterize the HOMO-LUMO overlap as well as the delocalization of HOMO and LUMO respectively, all calculated data are collected in Table III. Furthermore, we analyze the electron-donating ability (Δ) due to its role in determining the molecular orbital properties. Relationship between S and Δ is shown in FIG. 4. An inversely proportional relationship is graphed, namely, the stronger the electron-

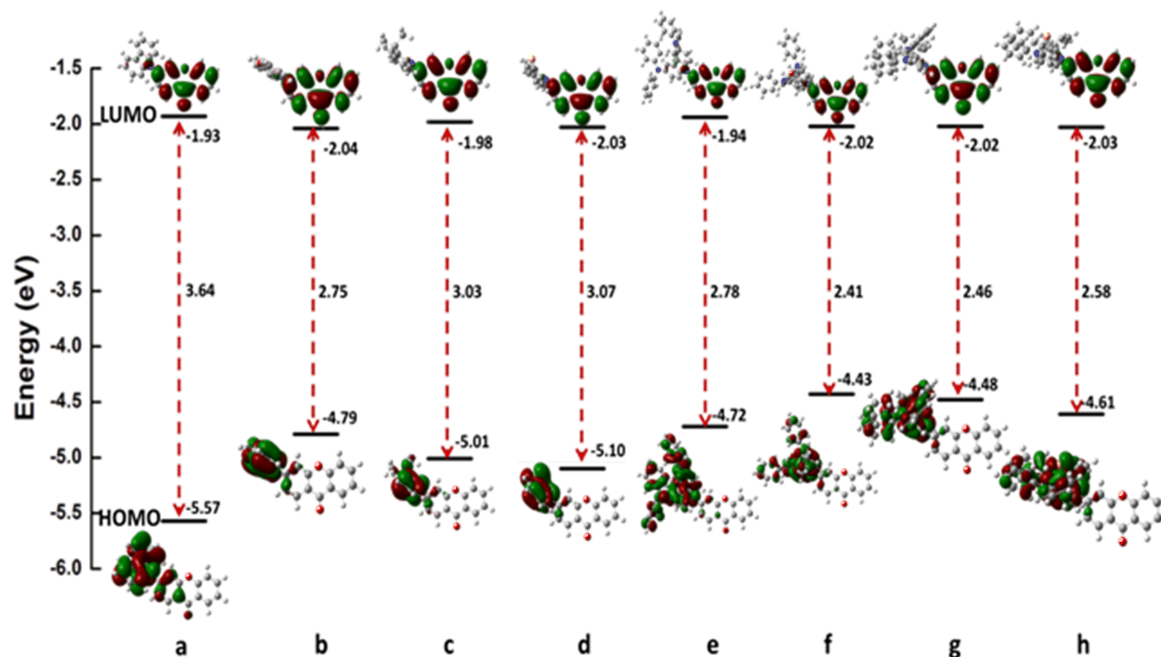


FIG. 3 Calculated energy levels, energy gaps (in eV), and orbital composition distributions of the HOMO and LUMO for all molecules (isovalue=0.02) .

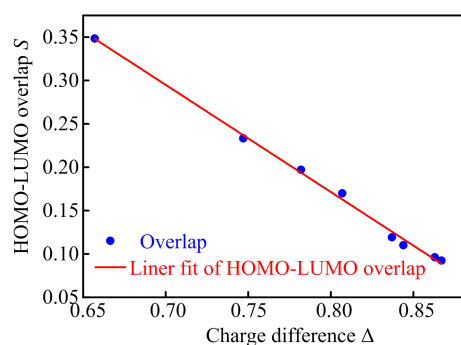


FIG. 4 Relationship between charge difference (Δ) and HOMO-LUMO overlap (S).

donating ability is, the smaller the HOMO-LUMO overlap is. Through comparing the value of δ_{hole} for later four molecules with the former four molecules, the value of δ_{hole} is increased when diphenylamine is added in donor unit, so the later four molecules possess larger delocalization of HOMO. For the former four molecules, the δ_{electron} decreases ((a)>(b)>(c)>(d)) with the donating ability increases ((a)<(b)<(c)<(d)). While for the later four molecules, similar condition is found with the donating ability is (g)≡(h)>(f)>(e) and the δ_{electron} is (h)≡(g)<(f)<(e). Thus, an effective way to decrease $\Delta E_{S_1-T_1}$ is illustrated that either to increase the electron donating ability or enlarge the delocalization of HOMO can bring a small $\Delta E_{S_1-T_1}$.

In order to determine the dominant factor in decreasing the $\Delta E_{S_1-T_1}$, relationship between HOMO-LUMO

overlap, delocalization of molecular orbital and $\Delta E_{S_1-T_1}$ is analyzed. Values of $\Delta E_{S_1-T_1}$ for all studies molecules are calculated by TD-DFT method through optimizing excited state geometries, and the adiabatic excitation energies of S_1 and T_1 are corrected by zero point vibrational energy (ZPVE). All data are collected in Table IV, and we elaborate the effect of HOMO-LUMO overlap and delocalization of HOMO on $\Delta E_{S_1-T_1}$. Comparing the value of S , δ_{hole} and $\Delta E_{S_1-T_1}$ between carbazole-XTN (a) and carbazole-II-XTN (e), DMAC-XTN (c) and DMAC-II-XTN (g) as well as PTZ-XTN (d) and PTZ-II-XTN (h), one know that the S is decreased, while the δ_{hole} is increased for molecules with diphenylamine added in donor unit, and a decreased $\Delta E_{S_1-T_1}$ is obtained. While for PXZ-XTN (b) and PXZ-II-XTN (f), S and δ_{hole} are all increased, and a decreased $\Delta E_{S_1-T_1}$ is also found. This means that the additional diphenylamine in donor part can decrease $\Delta E_{S_1-T_1}$. Through above-mentioned comparisons, we can come to the conclusion that the enlarge delocalization of molecular orbitals with large separation between HOMO and LUMO can bring a small $\Delta E_{S_1-T_1}$.

C. Transition properties

In order to investigate the electronic transition nature of all studied compounds, TD-DFT calculations are performed based on their optimized S_0 states. The vertical excitation energy of S_1 ($E_{\text{VA}}(S_1)$), T_1 ($E_{\text{VA}}(T_1)$) and their gaps (E_{vert}) as well as the adiabatic excitation energies of S_1 ($E_{0-0}(S_1)$), T_1 ($E_{0-0}(T_1)$) and their

TABLE IV Vertical excitation energies of S_1 ($E_{VA}(S_1)$), T_1 ($E_{VA}(T_1)$) and their gaps (E_{vert}) as well as their adiabatic excitation energies (with ZPVE correction) of S_1 ($E_{0-0}(S_1)$) and T_1 ($E_{0-0}(T_1)$) and their gaps ($\Delta E_{S_1-T_1}$).

| | $E_{VA}(S_1)$ | $E_{VA}(T_1)$ | E_{vert} | $E_{0-0}(S_1)$ | $E_{0-0}(T_1)$ | $\Delta E_{S_1-T_1}$ |
|------------------|---------------|---------------|------------|----------------|----------------|----------------------|
| Carbazole-XTN | 3.181 | 2.846 | 0.335 | 2.682 | 2.541 | 0.141 |
| PXZ-XTN | 2.220 | 2.178 | 0.042 | 1.909 | 1.895 | 0.014 |
| DMAC-XTN | 2.466 | 2.456 | 0.010 | 2.228 | 2.213 | 0.015 |
| PTZ-XTN | 2.543 | 2.533 | 0.010 | 1.993 | 1.980 | 0.013 |
| Carbazole-II-XTN | 2.453 | 2.334 | 0.119 | 1.976 | 1.969 | 0.007 |
| PXZ-II-XTN | 1.962 | 1.897 | 0.065 | 1.535 | 1.523 | 0.012 |
| DMAC-II-XTN | 2.019 | 2.013 | 0.006 | 1.714 | 1.704 | 0.010 |
| PTZ-II-XTN | 2.137 | 2.130 | 0.007 | 1.652 | 1.641 | 0.011 |

TABLE V Spin-orbit coupling constants (cm^{-1}) between S_1 and T_1 for studied molecules.

| | $\langle S_1 \hat{H}_{so} T_1 \rangle$ |
|------------------|--|
| Carbazole-XTN | 1.750 |
| PXZ-XTN | 0.025 |
| DMAC-XTN | 0.020 |
| PTZ-XTN | 0.034 |
| Carbazole-II-XTN | 0.009 |
| PXZ-II-XTN | 0.013 |
| DMAC-II-XTN | 0.015 |
| PTZ-II-XTN | 0.020 |

gaps ($\Delta E_{S_1-T_1}$) are all collected in Table IV. Results show that the value of E_{vert} is inversely proportional to electron-donating ability, the stronger the electron-donating ability is, the smaller the E_{vert} is. Moreover, we calculate the energy landscape of single and triplet states to determine the intersystem crossing and reverse intersystem crossing processes, and their transition properties are analyzed by natural transition orbital (NTO) method. As shown in FIG. 5, the energy of T_1 is lower than S_1 and no extra energy levels are found between them for studied molecules except for carbazole-XTN. S_1 and T_1 states all possess charge transfer (CT) properties which can facilitate the reverse conversion from T_1 to S_1 [33, 34]. For carbazole-XTN, T_2 and T_3 are also lower than S_1 , thus the ISC and RISC processes occur between S_1 and T_2 as well as S_1 and T_3 . Moreover, T_2 and T_3 possess localized excitation (LE) properties, this feature can also affect the ISC and RISC processes [35]. Corresponding data are shown in the following section.

D. ISC and RISC rates

As we all know, ISC and RISC processes play a crucial role in efficient TADF-OLEDs. Through above-mentioned results, we know that $\Delta E_{S_1-T_1}$ is largely dependent on the frontier orbital overlap and delocalization. The transition nature of S_1 and T_1 (T_2 or T_3)

TABLE VI The calculated intersystem crossing rate and reverse intersystem crossing rates for all molecules with the unit of s^{-1} .

| | ISC($S_1 \rightarrow T_1$) | RISC($T_1 \rightarrow S_1$) |
|------------------|------------------------------|-------------------------------|
| Carbazole-XTN | 2.519×10^5 | 1.813×10^2 |
| PXZ-XTN | 2.709×10^6 | 3.321×10^5 |
| DMAC-XTN | 1.542×10^6 | 1.121×10^5 |
| PTZ-XTN | 6.124×10^6 | 1.261×10^6 |
| Carbazole-II-XTN | 3.048×10^5 | 1.666×10^5 |
| PXZ-II-XTN | 8.586×10^5 | 3.941×10^4 |
| DMAC-II-XTN | 1.348×10^6 | 1.886×10^5 |
| PTZ-II-XTN | 2.150×10^6 | 3.660×10^5 |

also plays an important role in achieving efficient ISC and RISC processes. In order to calculate the ISC and RISC rate parameters, spin-orbit coupling coefficients (H_{so}) between singlet and triplet states are acquired by Dalton 2013 package, corresponding data are collected in Table V. Further, the ISC and RISC rates between S_1 and T_1 are calculated by MOMAP package, and results are summarized in Table VI. From Table V and Table VI, one can see that H_{so} of carbazole-XTN between S_1 and T_1 is the biggest one (1.75 cm^{-1}) among all studied molecules, but the ISC and RISC rates are smaller than that of remainders, this is due to its large $\Delta E_{S_1-T_1}$ (0.141 eV). So we investigate the ISC and RISC processes between S_1 and T_2 as well as S_1 and T_3 for carbazole-XTN, and all data are summarized in Table VII. For carbazole-XTN, the spin-orbit coupling coefficients $\langle S_1 | \hat{H}_{so} | T_2 \rangle$ and $\langle S_1 | \hat{H}_{so} | T_3 \rangle$ are larger than that of $\langle S_1 | \hat{H}_{so} | T_1 \rangle$ with decreased adiabatic energy gap. However, the ISC and RISC rates between S_1 and T_3 are comparable with these between S_1 and T_1 , this is related to the LE transition nature of T_3 . Gibson and Penfold found that ^3LE often brings a stable triplet state while ^3CT can promote the reverse conversion from ^3CT to ^1CT [36]. Furthermore, we investigate the relationship between spin-orbit coupling coefficient H_{so} , $\Delta E_{S_1-T_1}$, and RISC rate for studied molecules except for the carbazole-XTN, corresponding results are shown in FIG. 6. A liner relationship

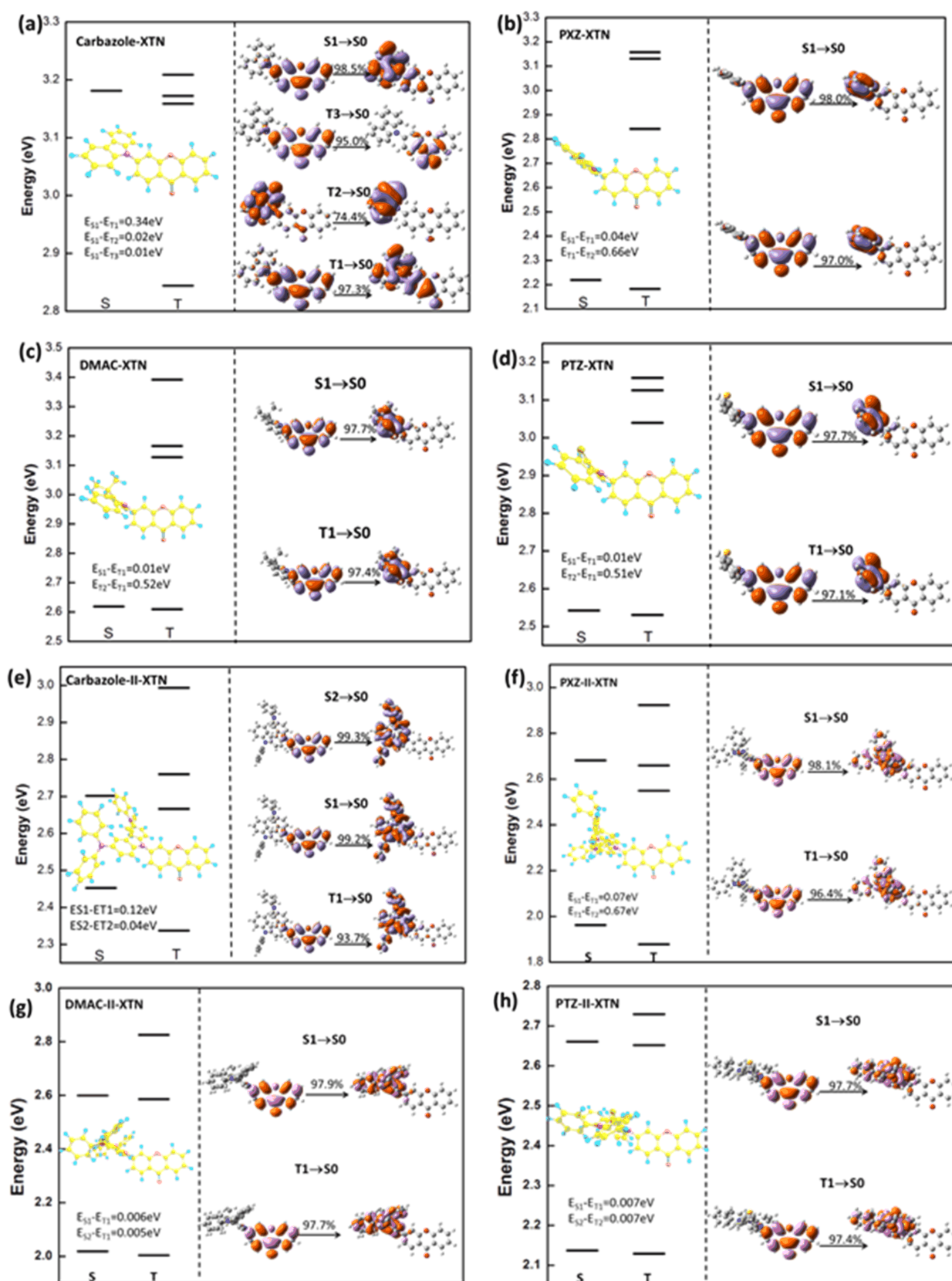


FIG. 5 The energy levels and molecular orbital characters of different excited states for all studied molecules. The value above every arrow represents the ratio in the corresponding transition.

TABLE VII Spin-orbit coupling constants $\langle S_1|\hat{H}_{so}|T_2\rangle$ and $\langle S_1|\hat{H}_{so}|T_3\rangle$ as well as the ISC and RISC rates are listed with the unit of s^{-1} .

| | | |
|---------------------------------------|------------------------------|-------------------------------|
| $\langle S_1 \hat{H}_{so} T_2\rangle$ | ISC($S_1 \rightarrow T_2$) | RISC($T_2 \rightarrow S_1$) |
| 5.888 | 1.339×10^6 | 3.434×10^5 |
| $\langle S_1 \hat{H}_{so} T_3\rangle$ | ISC($S_1 \rightarrow T_3$) | RISC($T_3 \rightarrow S_1$) |
| 2.307 | 8.274×10^3 | 7.296×10^2 |

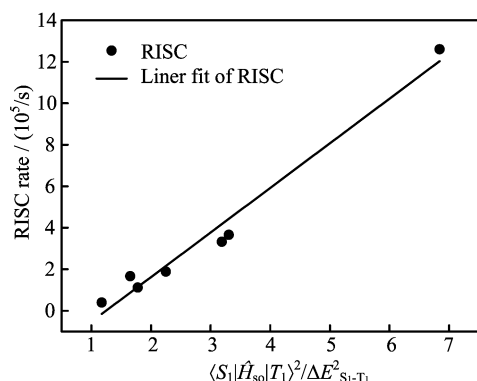


FIG. 6 Relationship between $\langle S_1|\hat{H}_{so}|T_1\rangle^2/\Delta E_{S_1-T_1}^2$ and RISC rate.

between $\frac{\langle S_1|\hat{H}_{so}|T_1\rangle^2}{\Delta E_{S_1-T_1}^2}$ and RISC rate is found. The physical meaning of $\frac{\langle S_1|\hat{H}_{so}|T_1\rangle^2}{\Delta E_{S_1-T_1}^2}$ can be understood to denote ability of the RISC process. Thus, not a small $\Delta E_{S_1-T_1}$ or a large spin-coupling coefficient but a large $\frac{\langle \Delta S_1|\hat{H}_{so}|T_1\rangle^2}{\Delta E_{S_1-T_1}^2}$ is the true factor to promote the RISC process.

IV. CONCLUSION

In this work, the electronic structures, molecular orbital properties, energy gaps, excitation properties and RISC process of all eight molecules are investigated by DFT and TDDFT methods. Through our investigations, the diphenylamine substitution in the donor unit has little effect on the dihedral angle between donor and acceptor unit, but can decrease the bond length between them except for the T_1 state of Carbazole-XTN. The electron donating ability, HOMO-LUMO overlap and frontier molecular orbital delocalization are quantitatively calculated. Results show that the overlap between HOMO and LUMO is decreased when the electron donating ability of donor groups is increased. As the diphenylamine groups are added in donor part, the delocalization of HOMO is enlarged, this brings a decreased energy gap between S_1 and T_1 state. Moreover, the spin-orbit coupling coefficient plays a significant role in realizing high efficient RISC process, large value

of $\frac{\langle S_1|\hat{H}_{so}|T_1\rangle^2}{\Delta E_{S_1-T_1}^2}$ can accelerate the exciton conversion from T_1 to S_1 . All our investigated molecules possess small $\Delta E_{S_1-T_1}$ and fast RISC rates, these molecules can be regarded as promising candidates for efficient TADF molecules. Furthermore, a wise molecular design strategy that enlarges the delocalization of frontier molecular orbitals with large separation between HOMO and LUMO, is proposed to achieve a small $\Delta E_{S_1-T_1}$.

V. ACKNOWLEDGMENTS

This work was supported by the National Natural Science Foundation of China (No.11374195 and No.21403133), the Taishan Scholar Project of Shandong Province, the Promotive Research Fund for Excellent Young and Middle-aged Scientists of Shandong Province (No.BS2014CL001), and the General Financial Grant from the China Postdoctoral Science Foundation (No.2014M560571). Great thanks to Professor Yi Luo at university of Science and Technology of China, Professor Zhi-gang Shuai at Tsinghua University and Qian Peng at Institute of Chemistry, Chinese Academy of Sciences for their helpful suggestions in our calculation. Thanks to Professor Ying-li Niu at Beijing Jiaotong University for his great help in the usage of MOMAP.

- [1] C. W. Tang and S. A. VanSlyke, *Appl. Phys. Lett.* **51**, 913 (1987).
- [2] J. H. Jou, S. Kumar, A. Agrawal, T. H. Li, and S. Sahoo, *J. Mater. Chem. C* **3**, 2974 (2015).
- [3] S. Xu, R. F. Chen, C. Zheng, and W. Huang, *Adv. Mater.* **28**, 9920 (2016).
- [4] C. Adachi, M. A. Baldo, M. E. Thompson, and S. R. Forrest, *J. Appl. Phys.* **90**, 5048 (2001).
- [5] Z. Kuang, X. Wang, Z. Wang, G. He, Q. Guo, L. He, and A. Xia, *Chin. J. Chem. Phys.* **30**, 259 (2017).
- [6] C. Li, L. Duan, D. Zhang, and Y. Qiu, *Acs. Appl. Mater. Inter.* **7**, 15154 (2015).
- [7] S. Cao, L. Hao, W. Y. Lai, H. Zhang, Z. Yu, X. Zhang, X. Liu, and W. Huang, *J. Mater. Chem. C* **4**, 4709 (2016).
- [8] H. Uoyama, K. Goushi, K. Shizu, H. Nomura, and C. Adachi, *Nature* **492**, 234 (2012).
- [9] J. Guo, X. L. Li, H. Nie, W. Luo, R. Hu, A. Qin, Z. Zhao, S. J. Su, and B. Z. Tang, *Chem. Mater.* **29**, 3623 (2017).
- [10] J. Guo, X. L. Li, H. Nie, W. Luo, S. Gan, S. Hu, R. Hu, A. Qin, Z. Zhao, S. J. Su, and B. Z. Tang, *Adv. Funct. Mater.* **27**, 1606458 (2017).
- [11] L. Yu, Z. Wu, C. Zhong, G. Xie, K. Wu, D. Ma, and C. Yang, *Dyes. Pigments.* **141**, 325 (2017).
- [12] J. Luo, S. Gong, T. Zhang, C. Zhong, G. Xie, Z. H. Lu, and C. Yang, *Dyes. Pigments.* **147**, 350 (2017).
- [13] T. Sato, M. Uejima, K. Tanaka, H. Kaji, and C. Adachi, *J. Mater. Chem. C* **3**, 870 (2015).

- [14] Q. S. Zhang, H. Kuwabara, W. J. Potscavage Jr., S. P. Huang, Y. Hatae, T. Shibata, and C. Adachi, *J. Am. Chem. Soc.* **136**, 18070 (2014).
- [15] J. Z. Fan, S. Qiu, L. L. Lin, and C. K. Wang, *Chin. J. Chem. Phys.* **29**, 291 (2016).
- [16] J. Fan, L. Cai, L. Lin, and C. Wang, *Chem. Phys. Lett.* **664**, 33 (2016).
- [17] M. Y. Wong and E. Zysman-Colman, *J. Mater. Chem. C* **29**, 1605444 (2017).
- [18] M. J. Frisch, G. W. Trucks, H. B. Schlegel, G. E. Scuseria, M. A. Robb, J. R. Cheeseman, G. Scalmani, V. Barone, B. Mennucci, G. A. Petersson, H. Nakatsuji, M. Caricato, X. Li, H. P. Hratchian, A. F. Izmaylov, J. Bloino, G. Zheng, J. L. Sonnenberg, M. Hada, M. Ehara, K. Toyota, R. Fukuda, J. Hasegawa, M. Ishida, T. Nakajima, Y. Honda, O. Kitao, H. Nakai, T. Vreven, J. A. Montgomery Jr., J. E. Peralta, F. Ogliaro, M. Bearpark, J. J. Heyd, E. Brothers, K. N. Kudin, V. N. Staroverov, R. Kobayashi, J. Normand, K. Raghavachari, A. Rendell, J. C. Burant, S. S. Iyengar, J. Tomasi, M. Cossi, N. Rega, N. J. Millam, M. Klene, J. E. Knox, J. B. Cross, V. Bakken, C. Adamo, J. Jaramillo, R. Gomperts, R. E. Stratmann, O. Yazyev, A. J. Austin, R. Cammi, C. Pomelli, J. W. Ochterski, R. L. Martin, K. Morokuma, V. G. Zakrzewski, G. A. Voth, P. Salvador, J. J. Dannenberg, S. Dapprich, A. D. Daniels, Ö. Farkas, J. B. Foresman, J. V. Ortiz, J. Cioslowski, and D. J. Fox, *Gaussian 16, Revision A.03*, Wallingford CT, USA: Gaussian Inc. (2016).
- [19] T. Lu and F. W. Chen, *J. Comput. Chem.* **33**, 580 (2012).
- [20] Dalton, a Molecular Electronic Structure Program, <http://daltonprogram.org>.
- [21] Y. L. Niu, Q. Peng, C. M. Deng, X. Gao, and Z. G. Shuai, *J. Phys. Chem. A* **114**, 7817 (2010).
- [22] Q. Peng, Q. H. Shi, Y. L. Niu, Y. P. Yi, S. R. Sun, W. Li, W. Q., and Z. G. Shuai, *J. Mater. Chem. C* **4**, 6829 (2016).
- [23] Q. Peng, Y. L. Niu, Q. H. Shi, X. Gao, and Z. G. Shuai, *J. Chem. Theory. Comput.* **9**, 1132 (2013).
- [24] T. Zhang, H. L. Ma, Y. L. Niu, W. Q. Li, D. Wang, Q. Peng, Z. G. Shuai, and W. Z. Liang, *J. Phys. Chem. C* **119**, 5040 (2015).
- [25] Z. G. Shuai and Q. Peng, *Phys. Rep.* **537**, 123 (2014).
- [26] J. Z. Fan, L. Cai, L. L. Lin, and C. K. Wang, *J. Phys. Chem. A* **120**, 9422 (2016).
- [27] J. Fan, L. Lin, and C. K. Wang, *J. Mater. Chem. C* **5**, 8390 (2017).
- [28] L. Lin, Z. Wang, J. Fan, and C. Wang, *Org. Electron.* **41**, 7 (2017).
- [29] J. Fan, L. Lin, and C. K. Wang, *Phys. Chem. Chem. Phys.* **19**, 30147 (2017).
- [30] J. Fan, L. Cai, L. Lin, and C. K. Wang, *Phys. Chem. Chem. Phys.* **19**, 29872 (2017).
- [31] X. C. Li, N. Sui, Q. H. Liu, Q. L. Yuan, and Y. H. Wang, *Chin. J. Chem. Phys.* **29**, 389 (2016).
- [32] Y. P. Wang, S. Zhang, S. m. Sun, K. Liu, and B. Zhang, *Chin. J. Chem. Phys.* **26**, 651 (2013).
- [33] M. K. Etherington, J. Gibson, H. F. Higginbotham, T. J. Penfold, and A. P. Monkman, *Nat. Commun.* **7**, 13680 (2016).
- [34] Y. Gao, S. Zhang, Y. Pan, L. Yao, H. Liu, Y. Guo, Q. Gu, B. Yang, and Y. Ma, *Phys. Chem. Chem. Phys.* **18**, 24176 (2016).
- [35] J. Gibson, A. P. Monkman, and T. J. Penfold, *ChemPhysChem* **17**, 2956 (2016).
- [36] J. Gibson and T. J. Penfold, *Phys. Chem. Chem. Phys.* **19**, 8428 (2017).